Original Article

Institution of MECHANICAL ENGINEERS
Journal of MECHANICAL ENGINEERING SCIENCE

Proc IMechE Part C:
J Mechanical Engineering Science
0(0) 1–13

DOI: 10.1177/0954406216633034
pic.sagepub.com
SAGE

Kinematic analysis and testing of a 6-RRR*P*RR parallel manipulator

Yang Yu[1,2,3], Zhen-bang Xu[2], Qing-wen Wu[2], Peng Yu[2], Shuai He[2] and Guo-qiang Wang[3]

Abstract

The Gough-Stewart platform has been successfully used in a wide variety of fields ranging from medical to automotive applications. This paper proposes a 6-RRR*P*RR parallel manipulator with orthogonal non-intersecting RR-joint configurations and ball screw actuators without guide mechanisms. A novel methodology is developed to define the dependent RR-joint variables and a numerical algorithm is employed to calculate the joint variables. The parasitic motion caused by the helical motion of the ball screw can be expressed and solved with vector method. The inverse kinematics of this manipulator can be solved. To verify the effectiveness of the proposed approach, simulations are performed with software package ADAMS. A prototype of this manipulator is manufactured. Its resolution, accuracy, and repeatability are measured. It is shown that the presented method is effective for this parallel manipulator.

Keywords

Parallel manipulator, inverse kinematics, parasitic motion, repeatability

Date received: 15 July 2015; accepted: 26 November 2015

Introduction

Parallel manipulators have significant advantages over conventional serial manipulators and this makes them attractive in various applications. These advantages include a greater stiffness and positioning capacity, excellent dynamic performance, and high load-carrying capacity. The parallel mechanism was originally proposed in a Gough machine to test the tires of an airplane[1]and in a Stewart machine as a flight simulator.[2] Hunt and Primrose[3] developed parallel architectures with potential applications in robotics. In recent decades, parallel manipulators are paid considerable attention and consequently theoretical research has made significant progress. Currently, parallel manipulators have a wide variety of applications in precision positioning,[4] medical surgery[5,6] high speed pick and place operations,[7] vibration isolation,[8] motion simulation,[9] underwater robotics,[10] nuclear facilities inspection,[11] and machining[12] to name a few.

Theoretical research in parallel mechanisms has grown rapidly in areas, such as mechanism configuration design[13] and solving of the forward and inverse kinematics.[14,15] Different configurations have also been proposed to obtain both translational and rotational motion, such as parallel manipulators with UPS,[16] PUS,[17] RPC,[18] and UPRR[19] kinematic architectures. In this paper, U, P, S, C, R, *P*, *C*, and *R* denote a universal joint, a prismatic joint, a spherical joint, a cylindrical joint, a revolute joint, an actuated prismatic joint, an actuated revolute joint, and a cylindrical joint, whose translational degree of freedom is actuated, respectively. Tsai[20] proposed a 3-UPU (Universal + Prismatic + Universal kinematic chain) parallel manipulator with a zero offset U-joint configuration and also presented its kinematics and optimum structure. Ji and Hu[21,22] studied a novel 3-RR*P*RR (Revolute + Revolute + Actuated Prismatic + Revolute + Revolute kinematic chain) parallel manipulator with pure translational movement. Dalvand and Shirinzadeh[23,24] studied a special 6-RR*C*RR (Revolute + Revolute + Actuated Cylindrical + Revolute + Revolute kinematic chain) parallel manipulator with an offset U-joint, and a novel approach for solving for the kinematic equations of this manipulator was proposed. Moreover, Liu et al.[25]comprehensively analyzed the inverse kinematics

[1]University of Chinese Academy of Sciences, Beijing, China
[2]Innovation Lab of Space Robot System, Changchun Institute of Optics, Fine Mechanics and Physics, Chinese Academy of Sciences, Changchun, Jilin, China
[3]School of Mechanical Science and Engineering, Jilin University, Changchun, China

Corresponding author:
Zhen-bang Xu, Changchun Institute of Optics, Fine Mechanics and Physics, Chinese Academy of Science, Changchun, China.
Email: xuzhenbang@gmail.com

and dynamics of a hydraulic driven 6-U*C*U parallel manipulator. Jaime et al.[26] also developed an approach to solve for the kinematics of a Stewart platform.

Various approaches to the computation of the direct kinematics have been presented in the literature.[27–29] Most of these approaches for obtaining the possible configurations can be categorized into either a closed-form analytical methods or numerical methods. The closed-form analytical methods formulate a symbolic equation or equation set with a single unknown variable by means of certain elimination. Merlet[30] dealt with closed-form resolution of the direct kinematic of parallel robot using extra sensors data. Husty[31] used a minimal set of constraint equations to produce the univariate polynomial to solve the direct kinematic. To avoid restriction of the geometry, numerical methods are also developed to solve the direct kinematic of parallel manipulators. For instance, Dalvand and Shirinzadeh[32]proposed an algorithm which employs an iterative technique to analyze a micromanipulator. The method can achieve accurate solutions with sufficient iterations of the algorithms, but may suffer from convergence problems and could possibly introduce high computational requirements.

In this paper, a 6-RR*RP*RR parallel manipulator is proposed that is composed of RR offset joints and an *RP* (Revolute + Prismatic kinematic chain) actuated joint. In this manipulator, The RR offset joint is an orthogonal non-intersecting universal joint. The *RP* actuated joint is a coupled joint composed of an actuated revolute and a parasitic prismatic joint that can be realized using a ball screw actuator without guide mechanism. Due to the uniqueness of this configuration, the modeling and solving of the kinematics differ from the other configurations that were stated above. Consequently, this paper develops a method which is composed of numerical method and vector analysis. Using this technique, the kinematic model of the 6-RR*RP*RR parallel manipulator can be obtained. To verify the effectiveness of the proposed methodology for the inverse kinematic analysis, simulations are performed. Following this, a prototype of this device is constructed and tested to practically validate the proposed methods.

The rest of this article is categorized into five sections. In the next section, the structure of this parallel manipulator is introduced. The associated kinematic models are developed and then the inverse kinematics and parasitic motion are solved. In Section 3, a case study is described and the kinematic model is validated with the aid of the software package ADAMS. The practical prototyping of the proposed manipulator is outlined in Section 4. The experimental tests of this prototype are detailed in Section 5, while concluding remarks are presented in Section 6.

Kinematics analysis

Description of the architecture

A 6-RR*RP*RR parallel manipulator, shown in Figure 1(a), is composed of a fixed base platform connected to a mobile platform with six actuators. These actuators enable the parallel manipulator to achieve translation and rotation in six degrees of freedom (DOF). The RR*RP*RR structure is showed in Figure 1(b). It is composed of a RR-joint separated with an offset L_{B_i}, an actuated revolute joint, and a parasitic prismatic joint (RP-joint), and another RR-joint with an offset L_{P_i}. For the 6-RR*RP*RR configuration, there are more advantages than traditional one. Compared with cross-universal joint (U-joint),

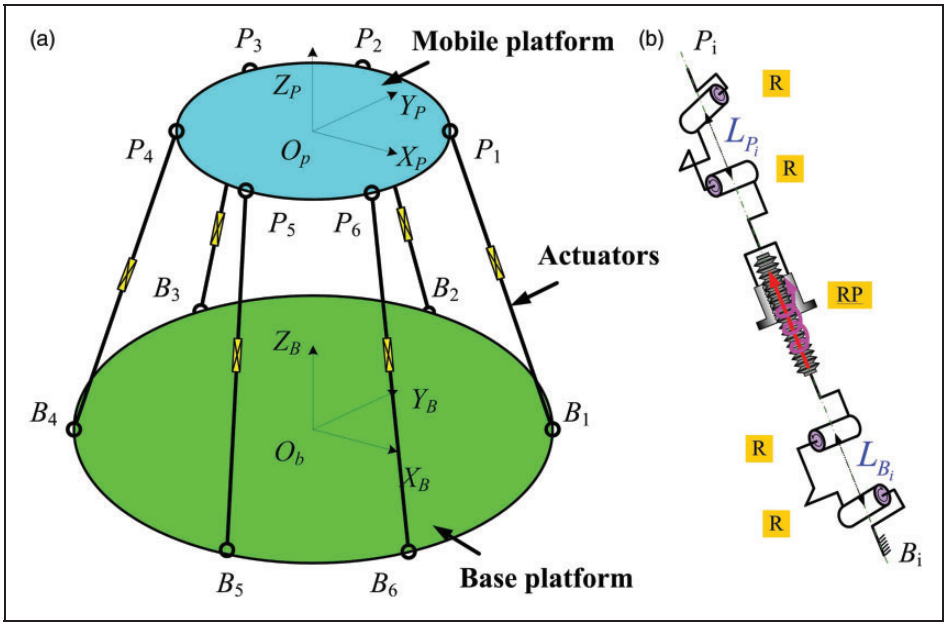

Figure 1. Structure of a 6-DOF parallel platform: (a) geometric model of a parallel platform and (b) the RR*RP*RR structure.

the RR-joint (which is an offset U-joint) is easier to manufacture with fewer geometric constraints. Due to the U-joint being replaced by two separate revolute joints, the workspace of the 6-RR*RP*RR manipulator is enlarged. Besides, the complicated bearing structure of the U-joint is replaced by a simple bearing structure of revolute joint, and so the RR-joint can provide twice as much stiffness as universal joints with crossed axes.[33] The RP-joint is a ball screw actuator without guide mechanisms which can be matched with the DOF of the parallel robot and realize the high precision motions. Based on the characteristics of two kinds of joints, the configuration of 6-RR*RP*RR can achieve high precision, high stiffness, and large workspace.

Kinematic modeling

Figure 2 shows the schematic diagram of the *i*th ($i=1,\ldots,6$) leg of the 6-RR*RP*RR parallel manipulator as well as the three-dimensional (3D) model of the five remaining legs assembled using two planar polygons representing the base and mobile platforms. The legs are attached to the base platform with a set of revolute joints whose axis center are points B_i forming a polygon. They are also attached to the moving platform with sets of revolute joints whose axis center are points P_i forming another planar polygon. Legs are distributed radially every 120° and the circumradii of the two polygons are R_B and R_P. The angles between the two adjacent legs of the same pair are given by the angles φ_B and φ_P. L_{B_i} and L_{P_i} are the distance between the two revolute axes of the offset joints. H_B and H_P are the distance from the center of the joints to the center of the platform. According to the structure of this manipulator, a reference frame $O_B - X_B Y_B Z_B$ which is attached to the fixed base platform and a mobile frame $O_P - X_P Y_P Z_P$ which is attached to the mobile platform are assigned. Owing to the existence of the RR-joint, two variables are added in each leg and hence the inverse kinematic equations cannot be easily solved by vector methods.

Similar to the approach used to solve the serial manipulator, the Denavit–Hartenberg (D–H) method is applied to establish the actual kinematic model. So local coordinate systems $B_i - X_{B_i}\ Y_{B_i} Z_{B_i}$ ($i=1,\ldots,6$) and $P_i - X_{P_i} Y_{P_i} Z_{P_i}$ ($i=1,\ldots,6$) are established, where the direction of X_{P_i} axes is from point O_P to point P_i and the direction of X_{B_i} axes is from point O_B to point B_i. Points C_i represent the other center points of the offset axis on the up joints, while points D_i represent the other center points of the offset axis on the down joints. The lengths of the *i*th actuator (L_i) are defined as the distance between points C_i and D_i. ψ_{B_i} is defined as the angle between the axes Y_{B_i} and the line $B_i D_i$, while ψ_{P_i} denotes the angles between the axes Y_{P_i} and the line $C_i P_i$.

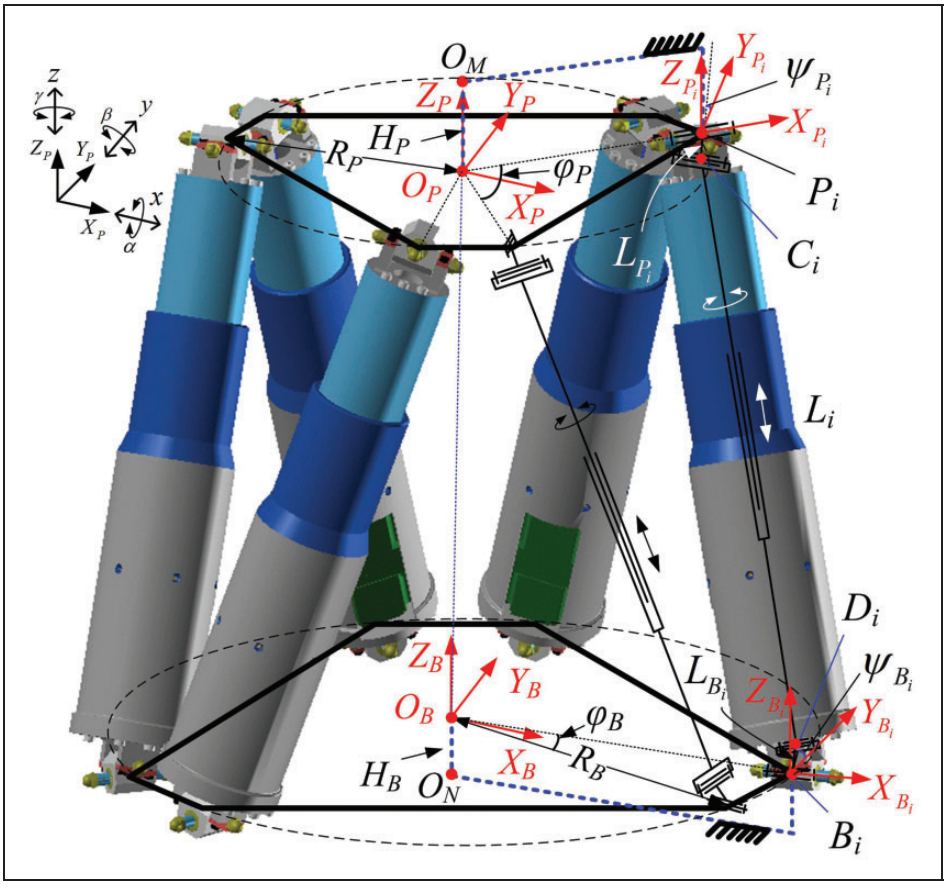

Figure 2. Schematic description of the *i*th leg of the 6-RR*RP*RR parallel manipulator.

Assuming the rigidity of the base and the mobile platforms as well as perfect assembly of the joints and actuators, the pose of the mobile platform is defined by a six-dimensional vector $[x, y, z, \alpha, \beta, \gamma]$. In this vector, the first three components are the coordinates of the frame $O_P - X_P Y_P Z_P$ in the reference frame $O_B - X_B Y_B Z_B$ and the last three components are parameters describing the orientation of the mobile platform. The symbols α, β, and γ are referred to as X-Y-Z fixed angles, and the order of the rotations must again accompany the angles to define the orientation. Taking the moving frame and the fixed frame to be initially coincident, α is the yaw about the fixed X_B axis, β is the pitch about the fixed Z_B axis, and γ is the roll rotation about the fixed Z_B axis. The homogeneous transformation matrix is ${}^{O_B}\boldsymbol{T}_{O_P}$ is as follows

$$ {}^{O_B}\boldsymbol{T}_{O_P} = \begin{bmatrix} c\gamma c\beta & c\gamma s\beta s\alpha - s\gamma c\alpha & c\gamma s\beta c\alpha + s\gamma s\alpha & x \\ s\gamma c\beta & s\gamma s\beta s\alpha + c\gamma c\alpha & c\gamma s\beta c\alpha - c\gamma s\alpha & y \\ -s\beta & c\beta s\alpha & c\beta c\alpha & z \\ 0 & 0 & 0 & 1 \end{bmatrix} \quad (1) $$

where ${}^{Y}T_{X}$ represents the transformation matrix from frame X to frame Y. And s and c denote sine and cosine functions, respectively.

Inverse kinematics analysis

To solve for the inverse kinematics of the proposed manipulator, the pose of the frame $O_P - X_P Y_P Z_P$ in the global frame $O_B - X_B Y_B Z_B$ $[x, y, z, \alpha, \beta, \gamma]$ is given and the leg lengths L_i need to be ascertained. Unlike conventional Stewart manipulators, the inverse kinematics of a 6-RRRPRR manipulator cannot be easily obtained by closed loop vector method and hence a numerical or iterative method is typically used. The existence of an offset between RR-joints in the parallel manipulator further complicates the calculation of the inverse kinematics solution. This offset results in highly non-linear and coupled equations that are more difficult to solve than equations of parallel manipulators with zero offset RR-joints (U-joints). RP-joint is a helical pair which is coupled with rotation and translation, the nut will move a pitch when the lead screw rotates 2π radians. Due to the coupling of the RP-joint and the existence of the offset joint variables, the kinematic equations of this configuration are further complicated. Referring to the D–H method, each branch leg of the parallel manipulator can be regarded as a series manipulator with six variables. The lengths of L_i can denote the distance between the points C_i and D_i. Using the mapping matrix of the frames $P_i - X_{P_i} Y_{P_i} Z_{P_i}$, $O_B - X_B Y_B Z_B$, $O_P - X_P Y_P Z_P$, and $B_i - X_{B_i} Y_{B_i} Z_{B_i}$, the actuator vectors can be derived as

$$ L_i = {}^{O_B}C_i D_i = {}^{O_B}\boldsymbol{T}_{O_P} \cdot {}^{O_P}\boldsymbol{T}_{P_i} \cdot {}^{P_i}C_i - {}^{O_B}\boldsymbol{T}_{B_i} \cdot {}^{B_i}D_i \quad (2) $$

while the coordinate of points C_i in the frame $P_i - X_{P_i} Y_{P_i} Z_{P_i}$ and the points D_i in the frame $B_i - X_{B_i} Y_{B_i} Z_{B_i}$ are given by

$$ {}^{B_i}\boldsymbol{C_i} = \begin{bmatrix} 0 & L_{P_i} \cdot c\psi_{P_i} & L_{P_i} \cdot s\psi_{P_i} & 1 \end{bmatrix}^T \quad (3) $$

$$ {}^{B_i}\boldsymbol{D_i} = \begin{bmatrix} 0 & L_{B_i} \cdot c\psi_{B_i} & L_{B_i} \cdot s\psi_{B_i} & 1 \end{bmatrix}^T \quad (4) $$

For any given pose of the mobile platform, the leg lengths L_i can be obtained by equation (2). However, the offset joint parameters ψ_{B_i} and ψ_{P_i} are unknown, which is difficult to solve the equation (2). According to the characteristics of the offset RR-joints, it is known that the lines $B_i D_i$ mapping on the planes $Y_{B_i} Z_{B_i}$ are always concurrent with the lines $B_i C_i$ orthogonally mapping on the same planes. In other words, the angles between axes Y_{B_i} and lines $B_i D_i$ are always identical to the angles between axes Y_{B_i} and the projection of lines $B_i C_i$ on the planes $Y_{B_i} Z_{B_i}$. Similarly, the angles between the axes Y_{P_i} and lines $P_i C_i$ are always equal to the angles between the axes Y_{P_i} and lines $P_i D_i$ projected upon the planes $Y_{P_i} Z_{P_i}$ as illustrated in Figure 2. Thus, it is possible to solve for these angles and L_i. Based on the above description, two sets of equations are given by

$$ \tan(\psi_{B_i}) = \frac{{}^{B_i}Z_{L_i}}{{}^{B_i}Y_{L_i}} \quad (5) $$

$$ \tan(\psi_{P_i}) = \frac{{}^{P_i}Z_{L_i}}{{}^{P_i}Y_{L_i}} \quad (6) $$

where ${}^{B_i}Z_{L_i}$ and ${}^{B_i}Y_{L_i}$ are the Y and Z components of the direction vector of the lines ${}^{B_i}C_i D_i$, while ${}^{P_i}Z_{L_i}$ and ${}^{P_i}Y_{L_i}$ are the Y and Z components of the direction vector of the lines ${}^{P_i}C_i D_i$.

According to equations (2) to (4), the lines ${}^{B_i}C_i D_i$ and ${}^{P_i}C_i D_i$ can be derived as

$$ {}^{B_i}C_i D_i = {}^{B_i}\boldsymbol{T}_{O_B} \cdot {}^{O_B}\boldsymbol{T}_{O_P} \cdot {}^{O_P}\boldsymbol{T}_{P_i} \cdot {}^{P_i}C_i - {}^{B_i}D_i \quad (7) $$

$$ {}^{P_i}C_i D_i = {}^{P_i}C_i - {}^{P_i}\boldsymbol{T}_{O_P} \cdot {}^{O_P}\boldsymbol{T}_{O_B} \cdot {}^{O_B}\boldsymbol{T}_{B_i} \cdot {}^{B_i}D_i \quad (8) $$

while all of the vectors ${}^{B_i}Z_{L_i}$, ${}^{B_i}Y_{L_i}$, ${}^{P_i}Z_{L_i}$, and ${}^{P_i}Y_{L_i}$ contain the angles ψ_{P_i} and ψ_{B_i}. So equations (5) and (6) can be noted as

$$ \frac{\sin(\psi_{B_i})}{\cos(\psi_{B_i})} = \frac{a_4 \cdot \sin(\psi_{P_i}) + a_5 \cdot \cos(\psi_{P_i}) + a_6 \cdot \sin(\psi_{B_i})}{a_1 \cdot \sin(\psi_{P_i}) + a_2 \cdot \cos(\psi_{P_i}) + a_3 \cdot \cos(\psi_{B_i})} \quad (9a) $$

$$ \frac{\sin(\psi_{P_i})}{\cos(\psi_{P_i})} = \frac{b_4 \cdot \sin(\psi_{B_i}) + b_5 \cdot \cos(\psi_{B_i}) + b_6 \cdot \sin(\psi_{P_i})}{b_1 \cdot \sin(\psi_{B_i}) + b_2 \cdot \cos(\psi_{B_i}) + b_3 \cdot \cos(\psi_{P_i})} \quad (10a) $$

where a_i, $b_i (i = 1, \ldots, 6)$ are constant parameters from the unfolded equations.

Expanding equations (9a) and (10a) yields two sets of non-linear equations:

$$s\psi_{B_i}\cdot\left(a_1\cdot s\psi_{P_i}+a_2\cdot c\psi_{P_i}+a_3\cdot c\psi_{B_i}\right)-c\psi_{B_i}\cdot\left(a_4\cdot s\psi_{P_i}+a_5\cdot c\psi_{P_i}+a_6\cdot s\psi_{B_i}\right)=0 \tag{9b}$$

$$s\psi_{P_i}\cdot\left(b_1\cdot s\psi_{B_i}+b_2\cdot c\psi_{B_i}+b_3\cdot c\psi_{P_i}\right)-c\psi_{P_i}\cdot\left(b_4\cdot s\psi_{B_i}+b_5\cdot c\psi_{B_i}+b_6\cdot s\psi_{P_i}\right)=0 \tag{10b}$$

In order to solve these sets of equations, a numerical iterative technique based on the Newton–Raphson method is used. These functions are defined as follows

$$F_{B_i}\left(\psi_{B_i},\psi_{P_i}\right)=0 \tag{9c}$$

$$F_{P_i}\left(\psi_{B_i},\psi_{P_i}\right)=0 \tag{10c}$$

where F_{B_i} and F_{P_i} are left side of equations (9b) and (10b), respectively.

Then a set of numerical solutions is derived from the equations and can be expressed as

$$\begin{bmatrix}\psi_{B_i}\\ \psi_{P_i}\end{bmatrix}_{(n+1)}=\begin{bmatrix}\psi_{B_i}\\ \psi_{P_i}\end{bmatrix}_{(n)}-\begin{bmatrix}\frac{\partial F_{B_i}}{\partial\psi_{B_i}} & \frac{\partial F_{B_i}}{\partial\psi_{P_i}}\\ \frac{\partial F_{P_i}}{\partial\psi_{B_i}} & \frac{\partial F_{P_i}}{\partial\psi_{P_i}}\end{bmatrix}_{(n)}^{-1}\cdot\begin{bmatrix}F_{B_i}\\ F_{P_i}\end{bmatrix}_{(n)} \tag{11}$$

To obtain the solution to equation (11), the initial value of ψ_{B_i}, ψ_{P_i} ($\psi_{B_i}^0$, $\psi_{P_i}^0$) should be given. Then equation (11) is evaluated iteratively until an acceptable solution within the set convergence levels is obtained. Since there may be several solutions, and for the sake of high-speed real-time calculations, choosing suitable initial conditions close to the actual values of the variables ψ_{B_i} and ψ_{P_i} is vital. Due to the structure of the RR*RP*RR architecture, the angular parameters ψ_{B_i} are very close to the angles of lines B_iP_i projected upon the planes $Y_{B_i}Z_{B_i}$ with respect to axes Y_{B_i}. In a similar manner, the angles ψ_{P_i} are very close to the angles of lines P_iB_i projected upon the planes $Y_{P_i}Z_{P_i}$ to axes Y_{P_i}. In other words, it can be regarded that the RR*RP*RR architecture resembles a U*C*U architecture with zero offset. Therefore, these angles can be chosen as initial estimates for equation (11) and are derived as follows

$$\psi_{B_i}^0={}^{B_i}\psi_{B_iP_i}=\arctan\left(\frac{{}^{B_i}Z_{B_iP_i}}{{}^{B_i}Y_{B_iP_i}}\right) \tag{12}$$

$$\psi_{P_i}^0={}^{P_i}\psi_{P_iB_i}=\arctan\left(\frac{{}^{P_i}Z_{P_iB_i}}{{}^{P_i}Y_{P_iB_i}}\right) \tag{13}$$

where ${}^{B_i}Z_{B_iP_i}$ and ${}^{B_i}Y_{B_iP_i}$ are components of lines ${}^{B_i}B_iP_i$, while ${}^{P_i}Z_{P_iB_i}$ and ${}^{P_i}Y_{P_iB_i}$ are components of lines ${}^{P_i}P_iB_i$. Through equations (1) to (13), the inverse kinematics of this special family of 6-RR*RP*RR parallel micromanipulators can be solved preliminarily.

The solution of the inverse kinematics outlined in the above paragraphs considers the motion between the points C_i and D_i as a cylindrical pair, where the rotation and translation are independent of each other. For the 6-RR*RP*RR parallel manipulator, these actuators are composed of the ball screw pair in which the rotation and translation are coupled: when the rotation of the ball screw relative to the motor reaches 2π radians and the nut can move one pitch. Due to the coupling, the mobile platform will adjust the pose by itself with the command of the motor's encoder. This means that a parasitic motion will accompany the motion of the mobile platform. While the errors caused by the parasitic motion that are not sensed by the motor's encoder may be small, they still need to be considered to ensure precision motion. Therefore, the parasitic motion needs to be analyzed and solved.

The motion of the 6-RR*RP*RR parallel manipulator consists of two components. One is a servo motor's motion which is termed "active screw motion," while the other is called "passive screw motion" and is caused by the relative motion between the actuator and the platform. The real elongation of the actuators can be denoted as follows

$$\Delta L_i=\Delta\boldsymbol{l}_{i1}+\Delta\boldsymbol{l}_{i2} \tag{14}$$

where $\Delta\boldsymbol{l}_{i1}$ is an elongation caused by the active screw motion and $\Delta\boldsymbol{l}_{i2}$ is the elongation caused by the passive screw motion, ($i=1,\ldots,6$).

According to the architecture, the active screw motion can be controlled with the motor but the passive screw motion is a parasitic motion that needs to be compensated for.

In the Cartesian coordinate system, the vector of the *i*th leg in the 6-RR*RP*RR parallel manipulator is built as shown in Figure 3. The vector $\boldsymbol{b}_i$ and $\boldsymbol{c}_i$ denote the unit vector of the joints axis close to the actuator. The vector $\boldsymbol{a}_i$ and $\boldsymbol{c}_i$ represent the unit vector of the offset axes. It can be seen from the vector diagram that the angle caused by the parasitic motion can be expressed by the relative angle between the vector $\boldsymbol{b}_i$ and $\boldsymbol{c}_i$.

Based on the characteristics of the offset RR-joints, the relationship between the vectors can be obtained as follows

$$\boldsymbol{a}_i\perp\boldsymbol{b}_i\boldsymbol{c}_i\perp\boldsymbol{d}_i\boldsymbol{l}_i\perp\boldsymbol{c}_i\boldsymbol{l}_i\perp\boldsymbol{b}_i$$

where $\boldsymbol{l}_i$ is the unit vector of the leg lengths L_i and its directions point to the upper joint, ($i=1,\ldots,6$).

Based on the frame $O_B-X_BY_BZ_B$, the unit vector $\boldsymbol{a}_i$ and $\boldsymbol{d}_i$ can be expressed as

$$\boldsymbol{a}_i=\frac{\overrightarrow{C_iP_i}}{|C_iP_i|} \tag{15}$$

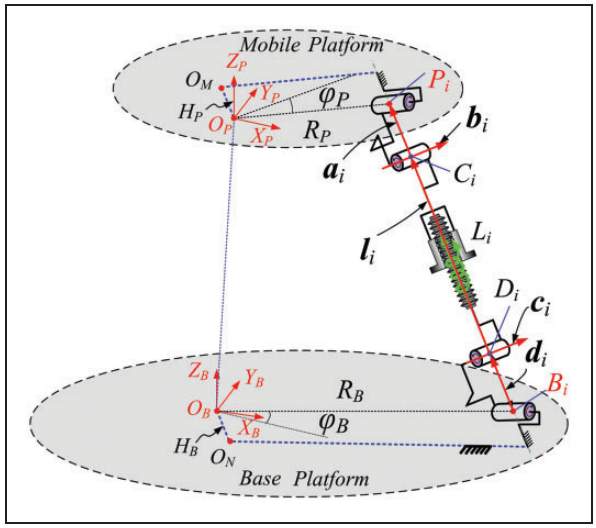

Figure 3. The vector diagram of the *i*th leg of the 6-RR*RP*RR parallel manipulator.

$$\boldsymbol{d}_i = \frac{\overrightarrow{B_iD_i}}{|B_iD_i|} \tag{16}$$

$$\overrightarrow{C_iP_i} = {}^{O_B}\boldsymbol{T}_{O_P} \cdot {}^{O_P}\boldsymbol{T}_{P_i} \cdot {}^{P_i}C_i - {}^{O_B}\boldsymbol{T}_{O_P} \cdot {}^{O_P}P_i \tag{17}$$

$$\overrightarrow{B_iD_i} = -{}^{O_B}\boldsymbol{T}_{B_i} \cdot {}^{B_i}D_i \tag{18}$$

where the coordinate of points C_i in the frame $P_i - X_{P_i}Y_{P_i}Z_{P_i}$ and the points D_i in the frame $B_i - X_{B_i}Y_{B_i}Z_{B_i}$ are denoted by equations (3) and (4)

Unit vectors $\boldsymbol{b}_i$ and $\boldsymbol{c}_i$ can be obtained by the cross-product as follows

$$\boldsymbol{b}_i = \boldsymbol{a}_i \times \boldsymbol{l}_i \tag{19}$$

$$\boldsymbol{c}_i = \boldsymbol{d}_i \times \boldsymbol{l}_i \tag{20}$$

The direction of the unit vectors of $\boldsymbol{b}_i$ and $\boldsymbol{c}_i$ can be determined by the following chart as shown in Figure 4. When the vectors $\boldsymbol{l}_i$ are located at the positive direction of the X_{P_i} axes in the frame of $P_i - X_{P_i}Y_{P_i}Z_{P_i}$, the vectors $\boldsymbol{b}_i$ are along the positive direction of the Y_{P_i} axes and vice versa. When the vectors $\boldsymbol{l}_i$ are located on the positive direction of the X_{P_i} axes in the frame of $B_i - X_{B_i}Y_{B_i}Z_{B_i}$, the vectors $\boldsymbol{c}_i$ are along the negative direction of the Y_{B_i} axes and vice versa.

Therefore, the included angles between the vector $\boldsymbol{b}_i$ and the vector $\boldsymbol{c}_i$ are

$$\theta_i = \arccos(\boldsymbol{b}_i \cdot \boldsymbol{c}_i) \tag{21}$$

It is also defined that the included angles are positive when the output struts rotate counterclockwise relative to the input struts as shown in Figure 5. On the contrary, the angle will be negative when the output struts rotate clockwise relative to the input struts. Then the relative angles $\Delta\boldsymbol{\theta}_i$ can be obtained as

$$\Delta\theta_i = (\theta_i - \theta_0) \cdot \frac{(\boldsymbol{b}_i \times \boldsymbol{c}_i) \cdot \boldsymbol{l}_i}{|(\boldsymbol{b}_i \times \boldsymbol{c}_i) \cdot \boldsymbol{l}_i|} \tag{22}$$

where $i = 1, \ldots, 6$ and $\boldsymbol{\theta}_0$ are the angle between vectors $\boldsymbol{b}_i$ and $\boldsymbol{c}_i$ when the mobile platform is located at the initial position.

Therefore, the elongation of each actuator caused by the parasitic motion can be expressed as

$$\Delta\boldsymbol{l}_{i2} = (-1)^n \frac{\Delta\theta_i}{2\pi} \cdot P \tag{23}$$

where P is the lead of the ball screw and n is designated as 1 when the ball screw is a left-handed screw, while n is designated as 2 when the ball screw is a right-handed screw.

Based on equations (14) to (23), the real extension of the leg lengths ΔL_i can now be obtained. Furthermore, the real pose of the mobile platform will be calculated with forward kinematic[23] and the software package ADAMS. The flow chart of the whole inverse kinematics is shown in Figure 6.

Validation

To verify the validity of the proposed solution for the inverse kinematic solution of the 6-RR*RP*RR parallel manipulator, an ADAMS model is built as shown in Figure 7. The RR*RP*RR kinematic chains include two passive RR-joints and one linear actuated RP-joint with two DOF. The RR-joints are represented as two revolute pairs and the RP-joint is realized by a helical pair and a cylindrical pair. Moreover, the driven motor is simulated with the joint motion module.

In order to analyze the effect of the parasitic motions, a case is studied with the following geometric parameters: $R_B = 175$ mm, $R_P = 125$ mm, $\varphi_B = 25^\circ$, $\varphi_P = 100^\circ$, $L_{B_i} = 5$ mm, $L_{P_i} = 5$ mm, $H_B = 30$ mm, $H_P = 30$ mm, $P = 2$ mm, and $n = 2$. The initial position of the frame $O_P - X_PY_PZ_P$ with respect to the frame $O_B - X_BY_BZ_B$ is located at [0, 0, 288 (mm), 0, 0, 0]. In the initial position, the actuator lengths are all 297.547 mm. The travel ranges of these linear actuators are 50 mm. For the case study of this manipulator, sinusoidal motions in six directions as shown in equation (24) to (29) are used to validate the parasitic motions.

$$\boldsymbol{x} = 10 \cdot \sin(0.1 \cdot \pi \cdot t) \text{ mm} \tag{24}$$

$$\boldsymbol{y} = 10 \cdot \sin(0.1 \cdot \pi \cdot t) \text{ mm} \tag{25}$$

$$\boldsymbol{z} = 10 \cdot \sin(0.1 \cdot \pi \cdot t) \text{ mm} \tag{26}$$

$$\boldsymbol{\alpha} = 10^\circ \cdot \sin(0.1 \cdot \pi \cdot t) \tag{27}$$

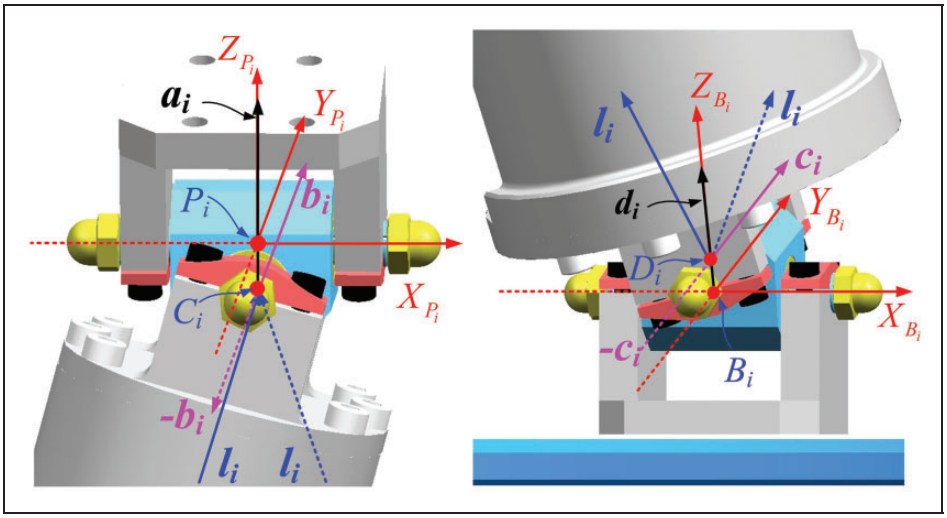

Figure 4. The direction judgment of the unit vector of b_i and c_i.

Vector direction	$b_i \times c_i$	$b_i \times c_i$
$(b_i \times c_i) \cdot l_i$	+	−

Figure 5. The directions of the relative angles.

$$\beta = 10^\circ \cdot \sin(0.1 \cdot \pi \cdot t) \tag{28}$$

$$\gamma = 10^\circ \cdot \sin(0.1 \cdot \pi \cdot t) \tag{29}$$

Through the computation of the inverse kinematic solution and the simulation of these sinusoidal motions, the incremental error of the actuator with time can be obtained as shown in Figure 8. The results show that the incremental errors are approximately 2.5 μm for 10 mm moves in the x and y axis, but is 0.6 μm in the z axis. It can also observe that for rotation within 10°, the z axis brings incremental errors with 60 μm compared with the x or y axis. Therefore, to get the ideal pose for motions with large displacements and angles, the parasitic motions must be compensated. Small displacement motions and large displacement motions are both analyzed.

The motions with small displacements and angles are investigated. Three arbitrary poses of the mobile platform with respect to the base platform are given. The ideal actuators lengths L_i can be obtained by using the MATLAB program, which is based on the 6-RR*C*RR configuration.[24] The uncompensated poses

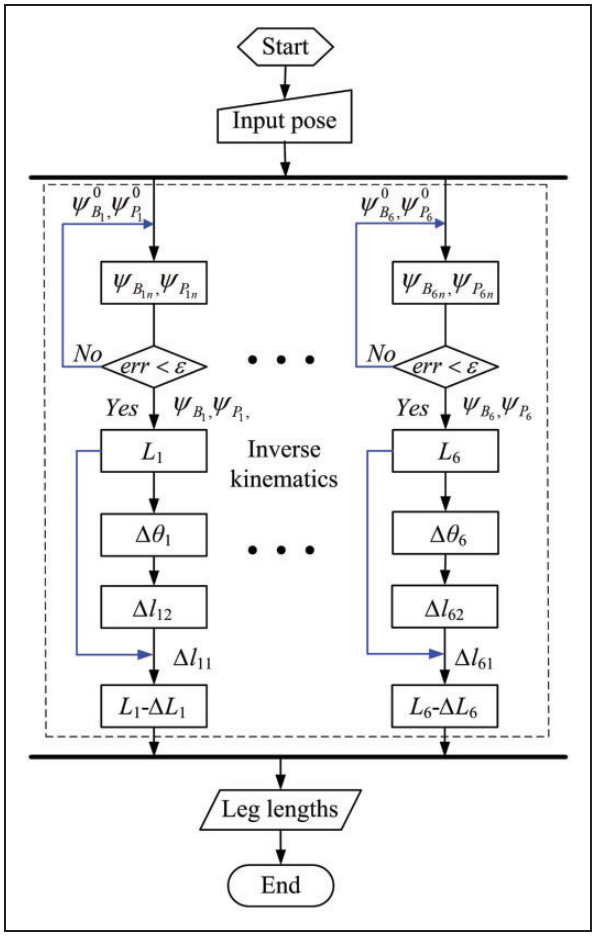

Figure 6. The flowchart for the inverse kinematic solution of the parallel manipulator.

can be developed by the forward kinematics which is carried out by the ADAMS software package. The simulation results, shown in Table 1, denote that the uncompensated poses have a difference of less than 3 nm compared with the given poses. This suggests

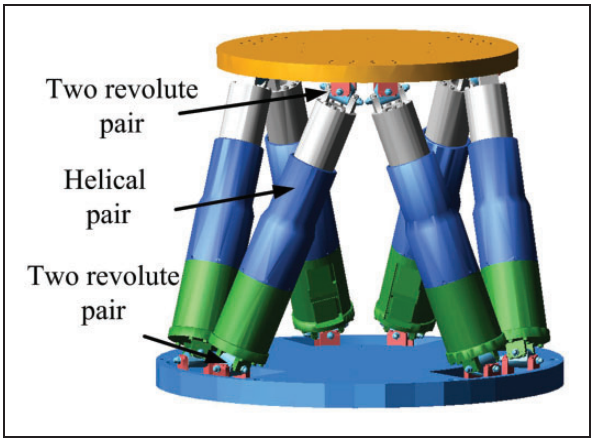

Figure 7. The kinematic pairs of the ADAMS model.

that the effect of parasitic motions with small displacements and angles is very small and can be ignored if desired.

The parasitic motion has almost no effect on the accuracy of the manipulator for small displacements and angles. However, the parasitic motion needs to be compensated for the motions with large displacements and angles as shown in Table 2. The results show that the uncompensated poses are different from the given poses with an error of up to 0.05 mm, which is significant for precision positioning. Importantly, the compensated poses match the given poses exactly. This demonstrates that the method of solving the inverse kinematics of the 6-RR*RP*RR parallel manipulator is effective.

Prototype

The prototype of the 6-RR*RP*RR parallel manipulator, shown in Figure 9, is composed of six actuators, the mobile platform, and the base platform. The accuracy of the manipulator depends on the accuracy of these actuators, while the design of the actuator is influenced by the load capacity, resolution, mechanical dimensional restriction, and speed of motion.[33,34] Considering these influences, the structure of the actuator can be realized using an AC servo motor and a precision ball screw. The resolution of the manipulator actuators is determined by the drive screw pitch and the encoder resolution. An absolute 17-bit encoder is used and a ball screw with 2 mm pitch is selected. It allows for high accuracy motion with an error less than 6 μm in a range of 300 mm. It should be noted that a preload nut is used to eliminate backlash as well as that the capacity of self-locking is needed and a brake is used behind the motor. The offset universal joints that use angular contact bearings are designed and built with the ideal characteristics of high stiffness, no backlash, and low friction.

Based on the ball screw pitch and encoder properties, the theoretical actuator's resolution could be as low as 19 nm. The maximum stroke is 50 mm which can be adjusted for different applications. Software limits, limit switches, and hard end stops are all used to prevent the strut from over travel. The maximum speed of the strut is 3 mm/s, but the speed should be reduced to 0.5 mm/s for continuous operation. The maximum speed and stroke can be increased by using a larger pitch of the ball screw, but the accuracy and resolution will suffer accordingly.

Experimental testing

Numerous tests are conducted to determine the resolution, positioning repeatability, the accuracy and stiffness of the parallel manipulator. In order to eliminate the effect of vibrations, the prototype is installed on a test bench as shown in Figure 10. The length gauge with an accuracy of 0.1 μm is used to measure the technical index and performance parameters.

The translational movements can be easily determined by measuring the coordinates of the sensor tip relative to the point O_M at the initial configuration along the x, y, and z axes. However, the rotational movements need to be indirectly measured with the method shown in Figure 11. The rotational angles can be obtained in accordance with geometric relations. For example, the angle $\delta\theta_x$ rotating around the x axis can be obtained by measuring the angular deviation between the x axis and a reference rod fixed on the mobile platform. Two length gauges can be used to implement the measurement and the corresponding equation can be denoted as

$$\delta\theta_x = \arctan\frac{\delta a - \delta b}{L} \tag{30}$$

where L is the horizontal distance between the two length gauge, and δa and δb are the variation in the length gauges.

Resolution

The resolution represents the minimum incremental motion of the mobile platform that can be repeatedly executed for a given input.[4] According to the results from the analysis of the parasitic motion, translation along the z axis and rotation around x and y axes are sensitive to errors and hence their resolutions need to be measured. The translational measurement along the z axis with 0.5 μm commanded movements is performed for 20 steps as illustrated in Figure 12. The rotational measurement around the x axis with 0.5 μrad commanded moves is measured by 20 steps as shown in Figure 13.

The test results show that the actual resolution along the z axis is 0.3 ± 0.11 μm and the rotational resolution around the x axis is 5 ± 0.97 μrad. The standard error obeys the principle of 1 sigma.[4] The reason for the non-uniform alteration of the

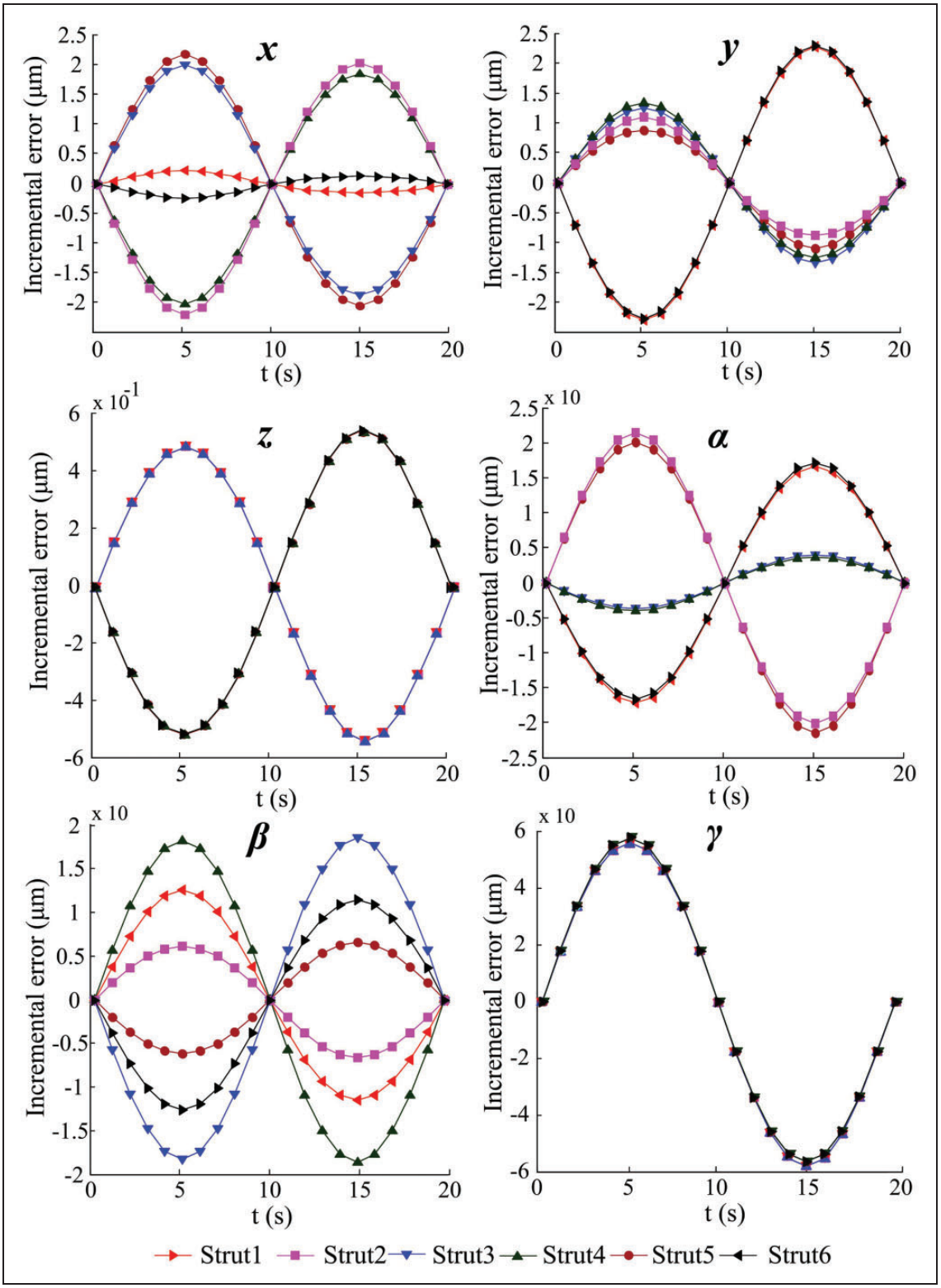

Figure 8. The incremental error in actuator lengths caused by the parasitic motion.

resolution may be caused by pitch errors in the ball screw and backlash or friction of the joints.

Positioning repeatability

Positioning repeatability represents the ability of the manipulator to return repeatedly to the same location.[35] A displacement of the manipulator along or around the y axis is selected for the analysis. The translational motion along the y axis within 1 mm is performed 20 times back and forth and the rotational motion around the y axis within 1° is tested 20 times back and forth. The results are shown in Figures 14 and 15.

Table 1. Comparison of poses with small displacement and angle motions.

	pose	x (μm)	y (μm)	z (μm)	α (μrad)	β (μrad)	γ (μrad)
Pose 1	**G**	−10.0000	−5.0000	−6.0000	0.0000	0.0000	0.0000
	U	−10.0016	−5.0002	−6.0000	0.0000	0.0000	0.0000
Pose 2	**G**	8.0000	−6.0000	−4.0000	5.0000	−3.0000	8.0000
	U	8.0015	−6.0002	−4.0006	5.0001	−3.0000	8.0000
Pose 3	**G**	−12.0000	5.0000	11.0000	−6.0000	5.0000	6.0000
	U	−12.0025	5.0012	11.0002	−6.0010	5.0010	6.0002

G: given pose; **U**: uncompensated pose.

Table 2. Comparison of the poses with large displacement or angle motions.

	pose	x (μm)	y (μm)	z (μm)	α (μrad)	β (μrad)	γ (μrad)
Pose 1	**G**	−12.0000	10.0000	5.0000	0.0000	0.0000	0.0000
	U	−11.9951	10.0054	5.0000	−0.0001	0.0000	0.0000
	C	−12.0000	10.0000	5.0000	0.0000	0.0000	0.0000
Pose 2	**G**	−6.0000	−8.0000	10.0000	−0.0698	−0.0474	−0.1745
	U	−6.0240	−7.9829	9.9482	−0.0598	−0.0637	−0.1745
	C	−6.0000	−8.0000	10.0000	−0.0698	−0.0474	−0.1745
Pose 3	**G**	11.0000	−5.0000	−12.0000	0.0698	−0.0524	−0.0698
	U	11.0192	−5.0209	−12.0206	0.0734	−0.0474	−0.0698
	C	11.0000	−5.0000	−12.0000	0.0698	−0.0524	−0.0698

G: given pose; **U**: uncompensated pose; **C**: compensated pose.

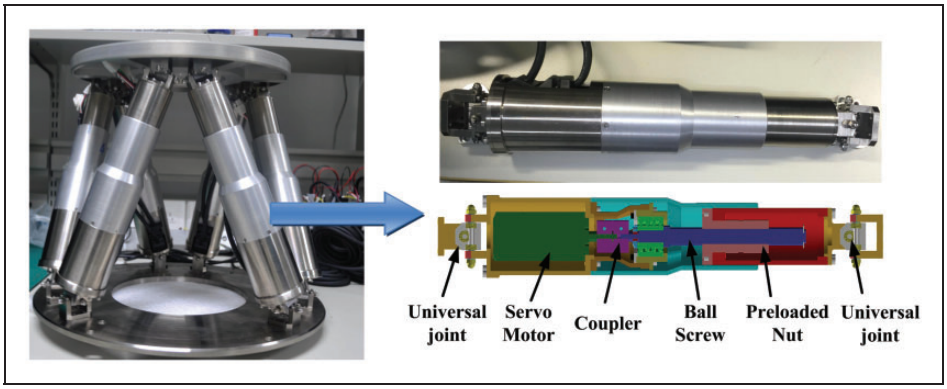

Figure 9. The photograph of the hexapod (left) and its actuator with cross-sectional view (right).

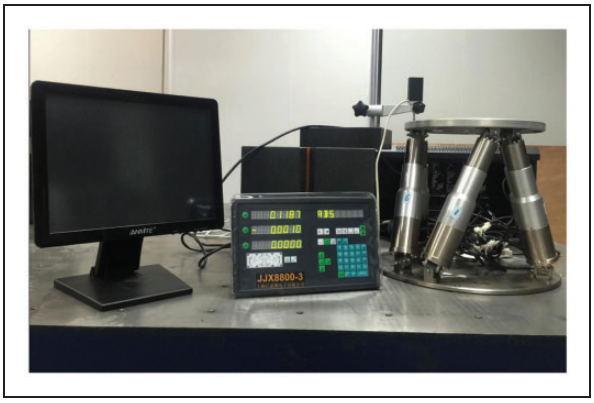

Figure 10. Test bench of the parallel manipulator.

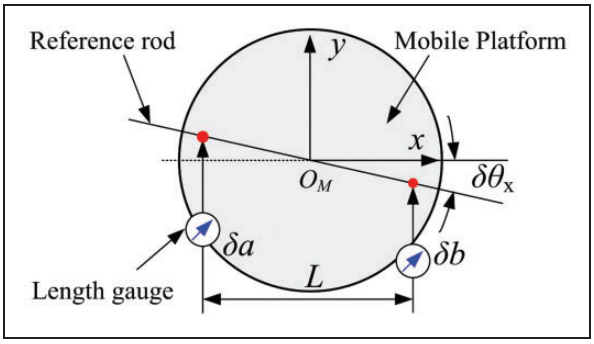

Figure 11. Measurement of $\delta\theta_x$.

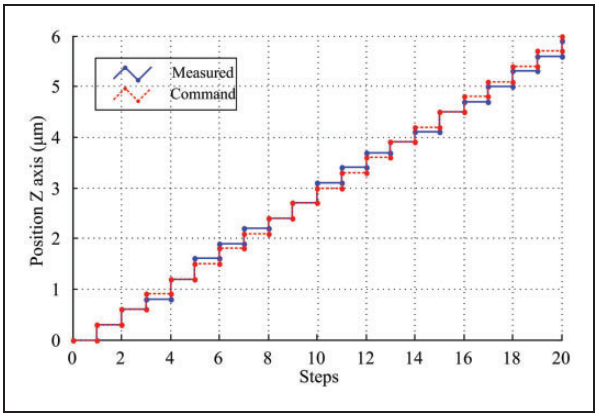

Figure 12. Translational resolution along the *z* axis.

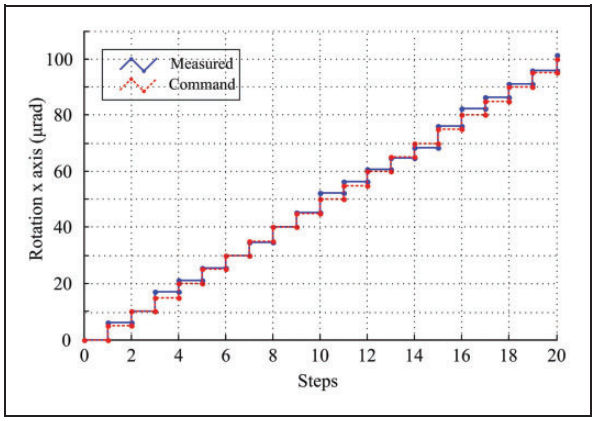

Figure 13. Rotational resolution around the *x* axis.

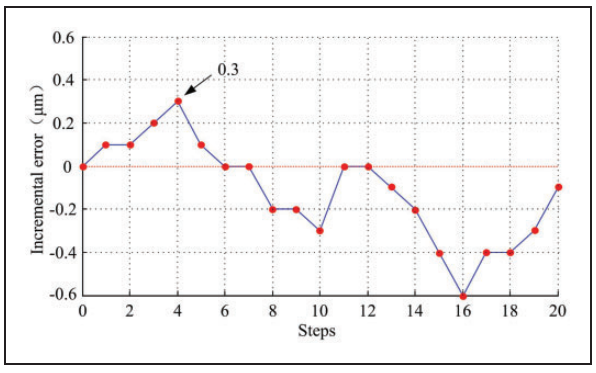

Figure 14. The translational repeatability along the *y* axis.

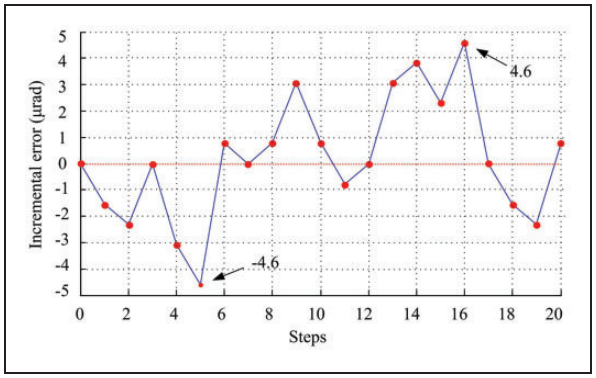

Figure 15. The rotational repeatability around the *y* axis.

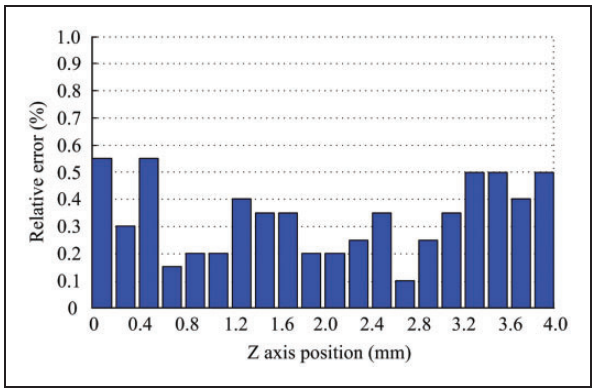

Figure 16. Accuracy testing results along the *z* axis for 200 μm movements.

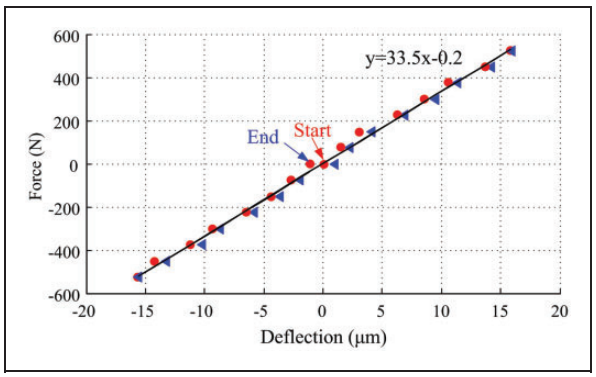

Figure 17. The stiffness of *z* axis.

The tests show that the unidirectional repeatability is better than ± 5 μrad in rotational DOF and better than ± 0.6 μm in translational DOF.

Relative accuracy

For tracking the trajectory of the parallel manipulator, the relative accuracy needs to be determined. The relative accuracy can be represented by a relative error which is defined as the ratio of the absolute error from its measurement.[36] The tests are conducted by moving 200 μm with one step. Figure 16 shows that the relative errors are approximately 0.6% for 200 μm movements along the *z* axis. The testing results of other axes show that the system can maintain relative accuracies within 1% in all six axes.

Stiffness

As an important factor in evaluating the effects of external forces on the displacement of the end-

effector, the stiffness should be considered for the analysis of the above-mentioned 6-RR*RP*RR parallel manipulator. In addition, when employed in precision positioning applications, the stiffness performance will have a significant effect on the accuracy of these manipulators.[16] The end-effector stiffness along the z axis is measured by reversing a 50 kg load from tension to compression while measuring the displacement of the mobile platform. The deflection of the mobile platform is measured by the grating length gauge and the stiffness can be obtained by Hooke's law. Figure 17 shows the measurement of the stiffness, where the red points represent the tension and the blue triangles represent the compression of the end-effector. For these test points, the stiffness can be obtained with the least square fitting method. Results reveal that the stiffness of this manipulator is approximately 33.5 N/μm and has good linearity.

Conclusions

In this work, a 6-RR*RP*RR parallel manipulator with offset joints and ball screw actuators without guide mechanisms has been studied and a solution to the inverse kinematics of this manipulator has been proposed. The characteristics of the offset joints were studied and a numerical algorithm was employed to obtain the dependent RR-joint variables. The parasitic motion caused by the helical motion of the ball screw was analyzed. This paper also provides simulation results to validate the proposed theoretical models. A prototype was constructed and tested on the workbench. Good performance and a high accuracy in the micron range have been obtained by the proposed solution to the inverse kinematics of this parallel manipulator. Further investigations on this 6-DOF parallel manipulator will focus on the development of positioning systems for secondary mirrors.

Declaration of conflicting interests

The author(s) declared no potential conflicts of interest with respect to the research, authorship, and/or publication of this article

Funding

The author(s) disclosed receipt of the following financial support for the research, authorship, and/or publication of this article: The author would like to acknowledge Project (11302222) supported by National Natural Science Foundation of China (NSFC) and Innovation Foundation of Changchun Institute of Optics, Fine Mechanics and Physics, Chinese Academy of Sciences No. Y4CX1SS141.

References

1. Gough V. Contribution to discussion of papers on research in automobile stability, control and tyre performance. *Proc Inst Mech EngAuto Div* 1956; 171: 392–395.
2. Stewart D. A platform with six degrees of freedom. *Proc Inst Mech Eng* 1965; 180: 371–384.
3. Hunt KH and Primrose EJF. Assembly configurations of some in-parallel-actuated manipulators. *Mech Mach Theory* 1993; 28: 31–42.
4. Physik-Instrumente. www.physikinstrumente.com/en/index.php (2015, accessed 15 July 2015).
5. Patel YD and George PM. Parallel Manipulators applications – a survey. *Mod Mech Eng* 2012; 2: 57–64.
6. Matthias W, Volker U, Thomas W, et al. A Stewart platform for precision surgery. *Transac Inst Measure Control* 2003; 25: 329–334.
7. Michael LP. *Workspace analysis of a linear delta robot: calculating the inscribed radius*. Master Thesis, Rose-Hulman Institute of Technology, US, 2014.
8. Yang JF, Xu ZB, WU QW, et al. Design of six dimensional vibration isolation system for space optical payload. *Optic Precis Eng* 2015; 23: 1347–1357.
9. Ngoc P, Kim JH and Kim HS. Development of a new 6-DOF parallel-kinematic motion simulator. In: *International Conference on control, automation and systems*, Seoul, Korea, 14–17 October 2008, pp.2370–2373. IEEE Conference.
10. Saltaren R, Garcia C, Avarez C, et al. Experiences and results from designing and developing a 6-DOF underwater parallel robot. *Robot Auton Syst* 2011; 59: 101–112.
11. Sabater J, Saltarén R, Aracil R, et al. Teleoperated parallel climbing robots in nuclear installations. *Ind Robot Int J* 2006; 33: 381–386.
12. Oscar A, Yon SM, Enrique A, et al. Motion pattern analysis of parallel kinematic machines: a case study. *Robot Comput Integr Manuf* 2009; 25: 432–440.
13. Bhaskar D and Mruthyunjaya TS. The Stewart platform manipulator: a review. *Mech Mach Theory* 2000; 35: 15–40.
14. Khalil W and Guegan S. Inverse and direct dynamic modeling of Gough-Stewart robots. *IEEE Transac Robot* 2004; 20: 754–761.
15. Ku DM. Forward kinematic analysis of a 6-3 type Stewart platform mechanism. *Proc IMechE, Part J: J Engineering Tribology* 2000; 214: 233–241.
16. Lian BB, Sun T, Song YM, et al. Stiffness Analysis and experiment of a novel 5-DoF parallel kinematic machine considering gravitational effects. *Int J Mach Tools Manuf*, Epub ahead of print 12 April 2015. DOI: 10.1016/j.ijmachtools.
17. Zhang D, Bi Z and Li B. Design and kinetostatic analysis of a new parallel manipulator. *Robot Comput Integr Manuf* 2009; 25: 782–791.
18. Jaime GA, Horacio OM, Alvaro SR, et al. Kinematic analyses of novel translational parallel manipulators. *Proc IMechE, Part C: J Mechanical Engineering Science* 2014; 228: 330–341.
19. Laski PA, Takosoglu JE and Blasiak S. Design of a 3-DOF tripod electro-pneumatic parallel manipulator. *Robot Auton Syst*, Epub ahead of print 9 April 2015. DOI: 10.1016/j.robot.
20. Tsai LW. Kinematics of a three-DOF platform with three extensible limbs. In: *International symposium on advances in robot kinematics*, Portoroz Bernardin, Slovenia, 22–26 June, 1996, pp.401–410. Netherlands: Springer.
21. Ji P and Wu HT. Kinematic analysis of an offset 3-UPU translational parallel robotic manipulator. *Robot AutonSyst* 2003; 42: 117–123.

22. Hu B and Lu Y. Analyses of kinematics, statics, and workspace of a 3-RRPRR parallel manipulator and its three isomeric mechanisms. *Proc IMechE, Part C: J Mechanical Engineering Science* 2008; 222: 1829–1837.
23. Dalvand MM and Shirinzadeh B. Forward kinematics analysis of offset 6-RRCRR parallel manipulators. *Proc IMechE, Part C: J Mechanical Engineering Science* 2011; 225: 3011–3018.
24. Dalvand MM and Shirinzadeh B. Inverse kinematics analysis of 6-RRCRR parallel manipulators. In: *IEEE/ASME international conference on advanced intelligent mechatronics*, Wollongong, Australia, 9–12 July 2013, pp.644–648. IEEE Conferences.
25. Liu GJ, Zheng ST, Peter O, et al. Inverse kinematic and dynamic analyses of 6-UCU parallel manipulator. *Appl Mech Mater* 2012; 127: 172–180.
26. Jaime GA, Horacio OM, Alvaro SR, et al. Kinematic analyses of novel translational parallel manipulators. *Proc IMechE, Part C: J Mechanical Engineering Science* 2014; 228: 330–341.
27. Merlet JP. Solving the forward kinematics of a Gough-type parallel manipulator with interval analysis. *Int J Robot Res* 2004; 23: 221–236.
28. Raghavan M. The Stewart platform of general geometry has 40 configurations. *ASME J MechDes* 1993; 115: 227–282.
29. Morell A, Tarokh M and Acosta L. Solving the forward kinematics problem in parallel robots using support vector regression. *Eng Appl Artif Intell* 2013; 26: 1698–1706.
30. Merlet JP. Closed-form resolution of the direct kinematics of parallel manipulator using extra sensors data. In: *IEEE international conference on Robotics and Automation*, Atlanta, 2–7 May 1993, pp.200–204. IEEE Conferences.
31. Husty M. An Algorithm for solving the direct kinematics of general Stewart-Gough platform. *Mech Mach Theory* 1996; 31: 365–380.
32. Dalvand MM and Shirinzadeh B. Kinematics analysis of 6-DOF parallel Micro-manipulators with offset U-joints: a case study. *Int J Intell Mechatron Robot* 2012; 2: 28–40.
33. Rainer G and Brian L. Challenges of extreme load hexapod design and modularization for large ground-based telescopes. *Proc SPIE* 2010; 7739: 1–11.
34. Michael C, Daniel B, Bernie J, et al. Practical considerations of joint friction and backlash in large ground-based telescope secondary optic pointing systems. *Proc SPIE* 2008; 7018: 1–12.
35. Victor S and Michael M. Mechanisms and actuation. In: K Waldron and J Schmiedeler (eds) *Handbook of robotics*. New York, NY: Springer, 2008, p.83.
36. Ryan CS, Michael FC, Trevor SC, et al. Six degree of freedom, sub-micrometer positioning system for secondary mirrors. *Proc SPIE* 2010; 7733: 1–11.